Energetically driven liquid–solid transitions in molecularly thin noctane films

R. K. Ballamudi and I. A. Bitsanis

Citation: The Journal of Chemical Physics **105**, 7774 (1996); doi: 10.1063/1.472560
View online: http://dx.doi.org/10.1063/1.472560
View Table of Contents: http://scitation.aip.org/content/aip/journal/jcp/105/17?ver=pdfcov
Published by the AIP Publishing

Energetically driven liquid–solid transitions in molecularly thin *n*-octane films

R. K. Ballamudi and I. A. Bitsanis[a)]
Department of Chemical Engineering, University of Florida, Gainesville, Florida 32611

(Received 22 September 1994; accepted 30 July 1996)

In this paper we present findings from molecular dynamics simulations that investigated the changes induced in molecularly thin *n*-octane films, as a result of increasing solid-methylene unit energetic affinity. The solid surfaces were deprived of any topographical features and were modeled as atomically smooth 10-4 Lennard–Jones planes. We observed an abrupt transition in the structural features of the film at a critical value of the characteristic energy that quantified the affinity between solid surfaces and methylene units. The transition was signaled by a discontinuous increase in the degree of intermolecular order and facilitated by a precipitous extension of the octane molecules, which adopted almost fully extended configurations. Furthermore, the transition resulted in the freezing of molecular migration and rotation. The characteristics of the transition showed that it is a mild first order phase transition between a highly ordered liquid and a poorly organized solid. The solid constitutes a phase with order intermediate to that of hydrocarbon ''rotator'' phases and two-dimensional smectics. These findings demonstrate that solidification of nanoscopically thin films of linear alkanes is a general, energetically driven phenomenon, which does not require the aid of commensurate surface topography. Our simulations provide a natural explanation for the solidlike features exhibited by alkane films studied experimentally. © *1996 American Institute of Physics.* [S0021-9606(96)02741-9]

I. INTRODUCTION

The structural features and rheological properties of nanoscopically thin films of short alkanes and other oligomeric lubricants can be drastically different from those of the corresponding bulk liquids. Understanding the origin of confinement induced changes is essential for rational material selection and efficient process design in diverse phenomena such as nanotribology, polymer extrusion (''melt fracture''), wetting and spreading of liquids, flow through microporous media, flocculation of colloids, and heterogeneous catalysis.[1,2]

Experimental advances during the last decade have made possible a much closer examination of interfacial systems and nanoscopically thin films. Shear flow experiments with the ''surface force apparatus'' [3–6] observed that such films of linear hydrocarbons consisting of fewer than 4–5 segmental or molecular layers would not flow until a critical (''yield'') stress was applied.[6–8] Squeezing flow surface force apparatus experiments reported a stepwise response similar to the peeling of discrete layers.[9] Squeezing flow experiments on very dense micellar solutions resulted in similar findings.[10,11] Scanning tunneling microscopy experiments detected highly ordered domains (microcrystallites) in monolayers of oligomers deposited on metal surfaces.[12,13]

Recent experimental studies underscored the sensitivity of thin film properties on the characteristics of the confining surfaces. Pressure drop-flowrate measurements in nanoscopic cylindrical nucleopores[14] reported only small quantitative deviations from bulk fluid behavior. These findings implied liquidlike mobility of the molecules immediately adjacent to the solid surface. A similar conclusion can be drawn from surface force apparatus measurements of normal forces between organically coated surfaces intermediated by a thin polymer melt film.[15] Furthermore, noticeably different rheological patterns were reported for thin films with molecules of the same chemical constitution but different architecture (linear versus branched).[6]

The microscopic origin of these phenomena was probed by numerous molecular simulations. The first simulation studies[16–18] were consistent with a ''liquidlike'' pattern of interfacial and thin film behavior. Subsequent studies stressed the importance of solid surface topography[19] and revealed the possibility of ''epitaxial'' crystallization, i.e., the development of solidlike features inside the layer immediately adjacent to the solid surface.[20]

Simulation of liquids consisting of short chain molecules[21,22] reported a sharp drop in intralayer self-diffusion. The whole phenomenon was described as ''glassification.'' These studies employed generic ''bead-spring'' models for the chain molecules, i.e., the chains were merely linear sequences of Lennard–Jones units connected by harmonic springs without any bend angle, or torsional potential constraints.

Other molecular dynamics simulations of *n*-octane films confined between atomically structured surfaces used more realistic models for the octane chains (bend angle potentials and torsional potentials).[23–25] Koopman *et al.*[25] reported the formation of highly ordered microdomains inside the layers immediately adjacent to the solid surfaces. The domains possessed the order of ''rotator'' hydrocarbon phases, were stable on the ns time scale, and their directionality was imposed by the underlying square solid matrix.

a)Author to whom correspondence should be addressed.

The combined findings of experiments and computer ''experiments'' have revealed a rich and diverse behavior of interfacial and confined liquid films. In some cases the behavior could be classified as liquidlike with only moderate differences from the bulk.[6,14–18] Other simulations and experiments suggested ''glassy'' features.[6,21,22] Finally, several experiments and simulations observed the development of solidlike features.[7,8,12,13,19,20,25]

The many factors that affect the properties of interfacial and thin films can be classified in four categories:

(1) thermodynamic conditions (temperature and pressure);
(2) energetics of the solid–liquid interaction;
(3) topography of the underlying solid substrate;
(4) architecture of the liquid molecules.

Clearly, the behavior of the film is determined by a complex interplay among all of these factors. Any attempt to ''tailor'' thin films with the desired type of behavior requires at least a qualitative understanding of the relative importance of each factor. The objective of this paper is to contribute toward reaching such a level of understanding. Our approach consists of isolating one among the above factors and studying its effect on the film's properties. Factors (1) and (2) (thermodynamic conditions and energetics) are easily quantifiable. Furthermore, there exists evidence that they are more important than factors related to surface topography. This seems to be a logical conclusion of the fact that solidlike thin film behavior was observed for a variety of liquids whose molecules were not particularly commensurate with the underlying solid substrate (cleavage plane of mica).

In order to accomplish our objective we opted to simulate thin films of *n*-octane confined between atomically smooth 10-4 Lennard–Jones surfaces under conditions of constant pressure and constant temperature. The choice of *n*-octane offers several advantages, since extensive data on bulk *n*-octane and wider films of the same liquid are available from previous simulation studies.[26,27] Furthermore, several experiments investigated films of short linear alkanes.[6–9]

The rest of this paper has been organized as follows: Section II describes the simulation method, conditions, and molecular models employed. Section III presents our findings and Sec. IV examines their implications. Finally, Sec. V provides a brief summary of the most important results reported in this paper.

II. THE MOLECULAR MODEL AND THE SIMULATION METHOD

In all simulations the octane films were confined between geometrically flat solid boundaries. The segment density normal to the surfaces always exhibited the typical oscillatory profile. The distance between the two surfaces was determined by the following two requirements: (a) the development of three methylene segment layers parallel to the surfaces and (b) the attainment of a desired value for the pressure normal to the solid surfaces. Furthermore, the temperature was kept very close to its prespecified value by velocity scaling (after equilibration, scaling was performed every 100 time steps). Therefore, our simulations were performed in a constant N,V,T ensemble (canonical). However, the fixed film thickness was chosen in a way that resulted in the selected value of the (normal) pressure. This implies that our films were at thermodynamic equilibrium with a bulk reservoir at the same temperature and a bulk pressure equal to the normal component of the pressure tensor inside the film (hence, film and bulk reservoir had the same chemical potential).

Our model for the octane chains was a standard one. It made use of the ''united atom'' approximation, according to which CH_2 and CH_3 groups were represented as identical, spherically symmetric entities without any atomic structure.[26] Explicit representation of the hydrogen atoms, or use of the ''anisotropic united atom'' potential leads to substantially improved predictions for the thermodynamic properties of bulk alkanes.[27] Nevertheless, such a level of accuracy is not commensurate to our representation of solid-segment interactions (to be discussed later).

The integrity of octane chains was maintained with the aid of three potentials:

- A harmonic potential controlling bond length fluctuations.[28]
- A harmonic potential controlling bend angle fluctuations.[28]
- A dihedral angle (torsional) potential[26] determining the height of the kinetic barriers for torsional transitions and the energy difference between trans and gauche states.

All the intramolecular potentials used in this work were smooth, i.e., there were no bend angle or bond length constraints.[28] The use of constrained bond lengths and/or bend angles can be justified only on grounds of computational convenience.[28,29] Constraints are known to produce artifacts[30] (especially the constraint on bend angles[29]) that require the introduction of a ''metric matrix.''[31] The relevance of the metric matrix approach to systems that do not follow noninertial Brownian dynamics and its effect on dynamical properties is not known.[32–34] On practical grounds, the computational benefit of constrained models is marginal[34] (about a factor of 2), and our past experience[24,25] showed that it may be reduced further by more ''daring'' choices of the time step length during smooth potential simulations.

Interactions between segments of different chains, as well as interactions between segments of the same chain separated by more than three bonds, were of the Lennard–Jones type

$$U(r/\sigma)=4\epsilon\{(r/\sigma)^{-12}-(r/\sigma)^{-6}\}, \tag{1}$$

where σ and ϵ are the usual length and energy parameters of the Lennard–Jones potential. These quantities were used as the units for length and energy. The value of the intersegment Lennard–Jones parameter for methyl and methylene units was 60.1 K.[24,25,35]

Since we opted to focus on the role of energetics and eliminate the influence of surface topography, surface-

TABLE I. Parameters of inter- and intra-molecular potentials.

		In MD units		In SI units		
			Intermolecular potential			
	ϵ	1.0		500	(J/mol)	60.1 K
	σ	1.0		3.9×10^{-10}	(m)	
	m	1.0		14.25	(g/mol)	
			Intramolecular potential			
	k^b	10 000	(ϵ/m^2)	3.46×10^{25}	(J/m^2/mol)	
	k^θ	1000	(ϵ)	50 000	(J/mol)	
	k^ϕ	16.4	(ϵ)	820	(J/mol)	
	b_0	0.39	(σ)	1.48×10^{-10}	(m)	
	θ_0			109.47^0		
	$\Delta E(t\leftrightarrow g)$	5.78	(ϵ)	2,892	(J/mol)	
			Kinetic barriers			
	$\Delta E^{\rm act}(t\leftrightarrow g)$	24.36	(ϵ)	12 178	(J/mol)	
	$\Delta E^{\rm act}(g^+\leftrightarrow g^-)$	88.37	(ϵ)	44 184	(J/mol)	
			Coefficients of torsional potential			
$a_0=1.116$	$a_1=1.462$	$a_2=-1.578$		$a_3=-0.368$	$a_4=3.156$	$a_5=-3.788$

segment interactions were modeled by a 10-4 Lennard–Jones potential:

$$U_{\rm sl}(z/\sigma_{\rm sl})=2\pi\rho_s\epsilon_{\rm sl}\{0.4(z/\sigma_{\rm sl})^{-10}-(z/\sigma_{\rm sl})^{-4}\}. \qquad (2)$$

In the above equation, z is the surface-segment distance, ρ_s is the number density of a solid layer, $\epsilon_{\rm sl}$ is the Lennard–Jones energy parameter for the interaction between segments and a (fictitious) surface atom, and $\sigma_{\rm sl}$ is the arithmetic average of the Lennard–Jones length parameters for segments and surface atoms. This potential results from integration (''smearing'') of the discrete interactions between surface ''atoms'' and segments over an entire solid layer.[36] After the smearing of solid atoms the resulting surface becomes perfectly smooth and lacks any topographical features. The ''smeared atoms'' constituting the smooth surface do not undergo any thermal motion, since incorporation of thermal motion is only meaningful for surfaces which possess topography on the atomic scale. The lack of motion of the ''smeared solid atoms'' renders their effective mass infinite compared with the mass of the atoms of the confined film. The 10-4 Lennard–Jones potential implies that the solid substrate is geometrically a flat plane. Therefore, $\sigma_{\rm sl}$, which would have determined the size of the crevices where the liquid molecules may or may not fit, does not play any such role in our case. It merely determines the distance at which the liquid molecules will hit the hard core of a one-dimensional potential which has no lateral variation. $\sigma_{\rm sl}$ was assigned the value of 1.0 in molecular dynamics units. The form of the solid-octane intermolecular potential [Eq. (2)] shows that only the product $\rho_s\epsilon_{\rm sl}$, not the individual factors, affects the simulation results (again this is a feature of atomically smooth surfaces). ρ_s was arbitrarily assigned the value of 1.0 in molecular dynamics units and the strength of solid-monomer adhesion was varied through the variation of $\epsilon_{\rm sl}$ alone. The values of the constants appearing in the intramolecular potentials, the segment–segment Lennard–Jones potential and the surface-segment potential are listed in Table I.

We performed simulations at two temperatures: 300.5 K and 360.6 K. At 300.5 K we simulated systems with a (normal) pressure close to 0 atm for the following values of the solid-segment energy parameter, $\epsilon_{\rm sl}$: 180.3 K, 240.4 K, 300.5 K, 360.6 K, 420.7 K, and 480.8 K. At the temperature of 360.6 K we simulated systems with a pressure close to 700 atm and $\epsilon_{\rm sl}$ values of 360.6 K, 540.9 K, 601 K, 661.1 K, and 721.2 K. Bulk octane is a liquid at both thermodynamic conditions studied in this work. Technical information on the various simulation runs is contained in Table II.

The preparation of well-equilibrated initial configurations is essential in simulations of dense liquids consisting of chain molecules. This was achieved by the method recently proposed by Gupta *et al.*[37] Subsequently the film thickness was varied slightly until the desired (normal) pressure was attained. After the (normal) pressure had reached the prespecified value and the system had sustained this pressure for at least 50 000 time steps (0.5 ns) production runs were initiated. The duration of these runs ranged from 50 000 to 300 000 steps (0.5 ns to 3.0 ns).

The equations of motion were integrated using Verlet's central difference algorithm with a time step of 0.004 62 in molecular dynamics units. Lists of nearest neighbors were employed to reduce computational costs.

III. SIMULATION RESULTS

In this section we examine the nature of the changes caused by the variation of solid–liquid affinity ($\epsilon_{\rm sl}$) under constant temperature (T) and normal pressure (P). The presentation of our simulation findings focuses on the properties that are best suited to reveal abrupt changes signaling phase transitions.

Liquid to solid phase transitions in bulk materials usually result in a modest increase of density upon solidification. Figure 1 shows the average density of the simulated *n*-octane films as a function of $\epsilon_{\rm sl}$ for the two different temperatures

TABLE II. Details of simulations performed.

ϵ_{sl} (K)	Film thickness (σ)	Periodic dimension (σ)	No. of octane chains	Temperature (K)	Time step ($m\epsilon/\sigma^2$)	No. of time steps	Average pressure (bar)
360.6	4.20	9	63	360.6	0.004 62	200 000	680
540.9	4.10	9	65	360.6	0.004 62	300 000	690
601.0	4.04	9	65	360.6	0.004 62	300 000	830
661.1	3.98	9	65	360.6	0.004 62	200 000	650
721.2	3.96	9	65	360.6	0.004 62	200 000	710
180.3	4.44	9	65	300.5	0.004 62	50 000	80
240.4	4.30	9	65	300.5	0.004 62	50 000	70
300.5	4.22	9	65	300.5	0.004 62	50 000	−90
360.6	4.08	9	65	300.5	0.004 62	200 000	120
420.7	4.05	9	65	300.5	0.004 62	50 000	70
480.8	4.02	9	65	300.5	0.004 62	100 000	−100

studied. Overall the shape of the curves in Fig. 1 is similar to typical high affinity absorption isotherms. A relatively abrupt densification occurs between the ϵ_{sl} values of 300.5 K and 360.6 K for the low temperature data. This feature seems to be too weak to be seen in the high temperature curve. Nevertheless, the foregoing discussion will show that there are convincing arguments in favor of its existence. Pressure fluctuations (which were kept below 50 bar) introduce the only source of noise in Fig. 1. An approximate estimate of the isothermal compressibility of our films shows that the corresponding noise level of our density data is about 1% in molecular dynamics density units.

Figure 2 contains the segment density profiles in the direction perpendicular to the solid surfaces. Note that the requirement of constant pressure results in a gradual decrease of the film thickness with increasing solid-segment affinity. The distance axis in Figs. 2(a) and 2(b) is symmetric with respect to the midplane of the films. In all systems studied the films consisted of three sharply defined segment layers. All density profiles were similar and exhibited the expected trends, i.e., a gradual sharpening and densification of segment layers with increasing ϵ_{sl} values.

The dependence of film structure on ϵ_{sl} was investigated in more detail by monitoring the evolution of the segment pair correlation functions. It is more informative to study intralayer pair correlation functions, i.e., to analyze separately the pair correlations inside the two layers adjacent to the solid surfaces and those in the middle layer. Figure 3 contains the intralayer pair correlation functions for the first layers at the various values of ϵ_{sl} simulated for $T=300.5$ K [Fig. 3(a)] and $T=360.6$ K [Fig. 3(b)]. Figure 4 presents the corresponding correlation functions for the middle layer. The

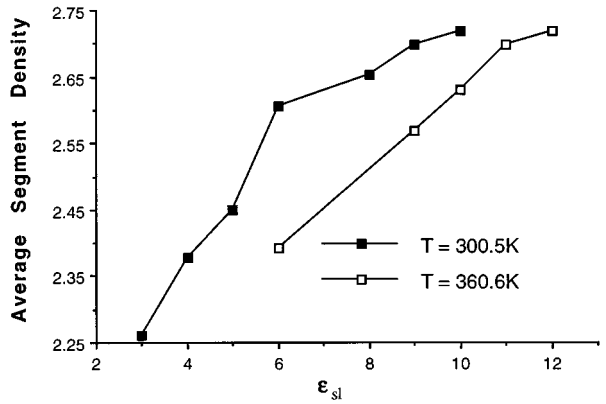

FIG. 1. Average film density (segments per unit volume) as a function of ϵ_{sl}.

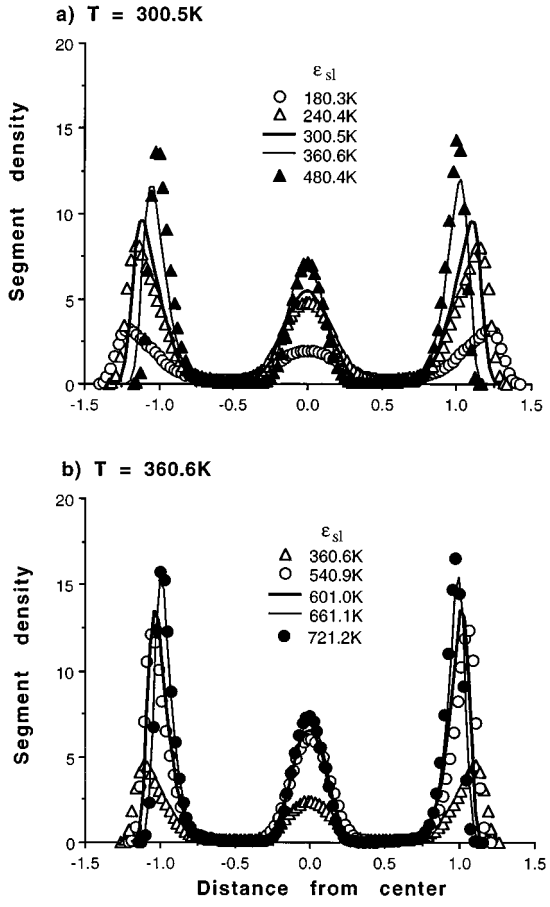

FIG. 2. Segment density profile normal to the surface. (a) Low temperature. (b) High temperature.

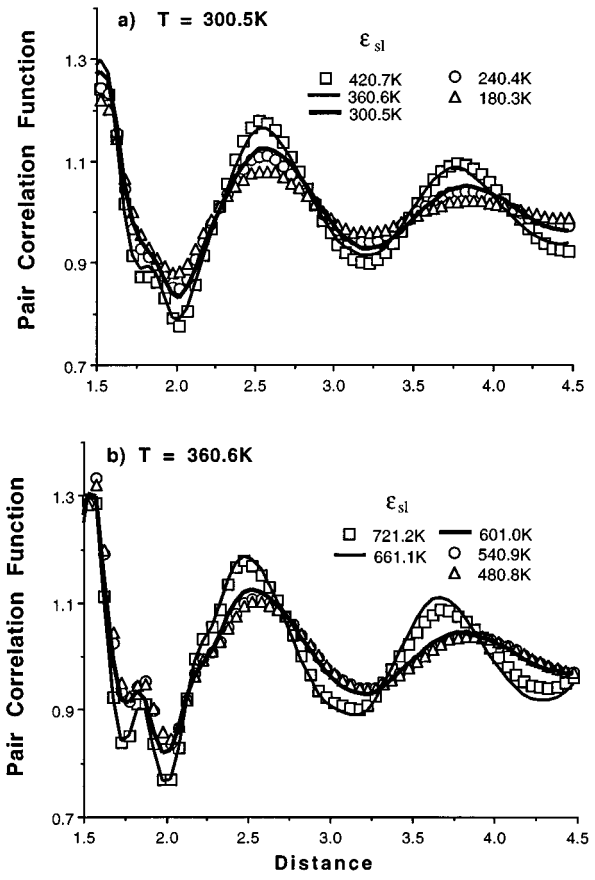

FIG. 3. In layer pair correlation function of the octane molecules in the first layer (next to the solid surface) at (a) $T = 300.5$ K and (b) $T = 360.6$ K. We see a discontinuous transition between $\epsilon_{sl} = 300.5$ K and $\epsilon_{sl} = 360.6$ K at $T = 300.5$ K and between ϵ_{sl}=601.0 K and $\epsilon_{sl} = 661.1$ K for $T = 360.6$ K.

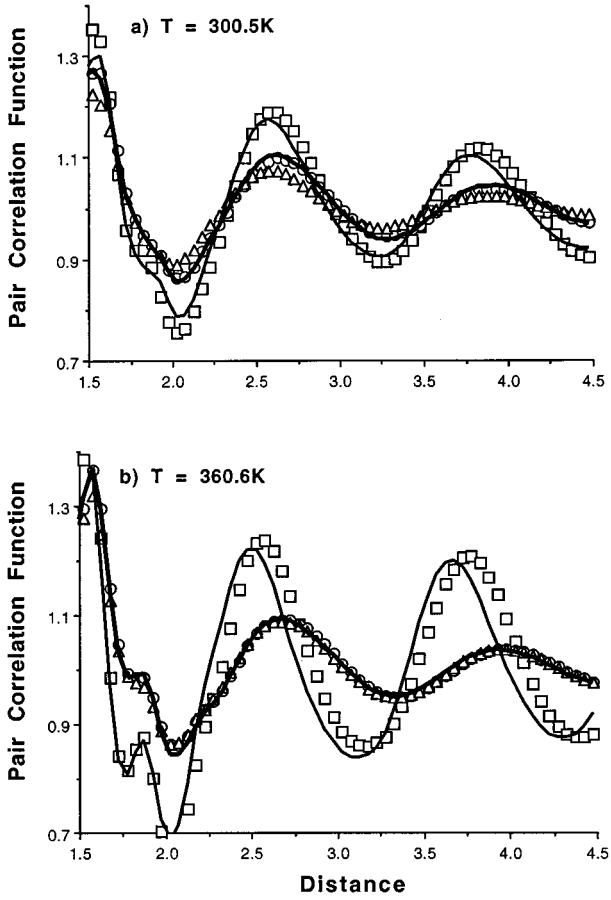

FIG. 4. Pair correlation function of the octane molecules at (a) T=300.5 K and (b) $T = 360.6$ K. Similar transition as in Fig. 3 is evident between the same values of ϵ_{sl}.

pair correlation function curves include two very large trivial peaks from the first and second nearest neighbors along the chain, as well as features related to 1–3 trans angle sequences. This initial part of the pair correlation functions (up to a distance of 1.5σ) would obscure the scale of the curves in Figs. 2 and 3 and has been omitted.

It is clear from Figs. 3 and 4 that the shape of the pair correlation functions of both first and middle layers undergoes an abrupt change at some critical ϵ_{sl} value (between 300.5 K and 360.6 K for the low temperature and between 601 K and 661.1 K for the high temperature). Abrupt changes in the shape of pair correlation functions are ''signatures'' of first order phase transitions. Usually, they are quantified by measures less detailed than the pair correlation function itself (e.g., the compressibility factor or the structure factor). However, these measures could be very sensitive to the system size. Therefore, they might be misleading in the case of molecular simulations, where the system size is microscopic.

We focus now on the portions of the pair correlation functions after a distance of about 2 segment diameters. These portions provide information on correlations among segments belonging to different octane chains. The central feature in the Figs. 3 and 4 is the abrupt change in the amplitudes of the second and third intermolecular neighbor peaks. Above a critical value of ϵ_{sl} these peaks are considerably stronger. This suggests regular packing of entire octane molecules, which would be possible only if the chains adopted extended, rodlike configurations.

The abrupt change in the shape of the pair correlation functions is linked to a sudden extension of the octane molecules. This can be seen from the change in the height and the intensity of the secondary peak corresponding to 4-trans angle sequences (i.e., fully extended octane molecules). Below the critical ϵ_{sl} values a shoulder (Fig. 3) or a small peak (Fig. 4) are visible in the pair correlation function curves.

The precipitous change in the shape of the pair correlation functions at the critical ϵ_{sl} values suggests a sharp rise in the fraction of trans torsional angles. This is shown clearly in Fig. 5, where this quantity is plotted versus solid-segment affinity (ϵ_{sl}). The change is more pronounced at the low temperature, where the fraction of trans angles jumps from 0.83 to 0.90 between ϵ_{sl}=300.5 K and 360.6 K. A milder, yet distinct transition can also be seen in the high temperature data between ϵ_{sl}=601 K and 661.1 K. Above the critical ϵ_{sl}

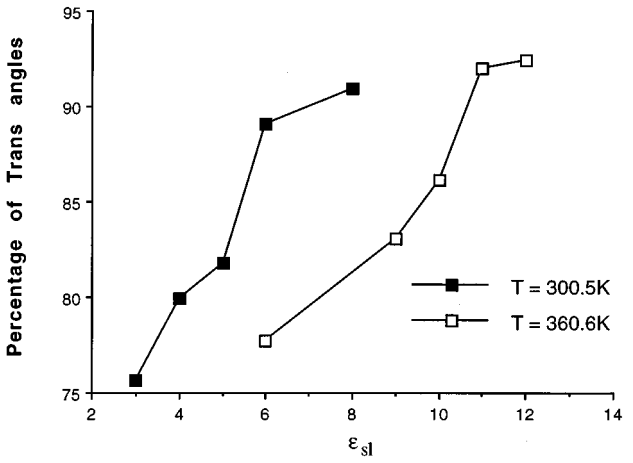

FIG. 5. The percentage of trans angles as a function of the parameter ϵ_{sl}. For $T=300.5$ K a sharp increase in the number of trans angles is evident between $\epsilon_{sl}=300.5$ K and $\epsilon_{sl}=360.6$ K. A similar increase can be seen between $\epsilon_{sl}=601.0$ K and $\epsilon_{sl}=661.1$ K for $T=360.6$ K.

values slightly more than 90% of the torsional angles are in a trans configuration, i.e., about half of the octane chains are fully extended, while the rest usually end up with a gauche sequence. Statistical analysis of subportions of our simulation trajectories shows that the statistical uncertainty in the percentage of trans angles is very low (less than $\pm 0.65\%$). There might also be a near systematic effect caused by the slight deviations of the pressure from the target values (0 and 700 bar).

The discontinuous structural changes are accompanied by a freezing of large scale molecular motions. The effect of solid-segment affinity on molecular mobility is best studied by monitoring the mean square displacement curves and the time correlation functions of the molecular end-to-end vector. The slope of the former is proportional to the translational self-diffusion coefficient, while that of the latter is proportional to the rotational diffusivity.

Figure 6 shows the segmental mean square displacement curves for the two temperatures studied in this work (300.5 K and 360.6 K). The time interval covered in these plots is about 0.2 ns, i.e., 5–20 times shorter than the duration of most simulation runs. As we can see from Figs. 6(a) and 6(b) large scale translation of segments, which can be attributed to diffusion of entire octane chains, ceases as we cross the critical ϵ_{sl} values (i.e., 300.5 K for the low temperature systems and 601 K for the high temperature systems).

Similarly, any significant rotation of octane chains stops at the same values of solid-segment affinity (see Fig. 7). Therefore, the structural transition manifested in Figs. 3, 4, and 5 has severe dynamical consequences, as it leads to an effective freezing of large scale molecular motions. Note that the final slope of the mean square displacement and rotational correlation function curves above the critical ϵ_{sl} values is too low to be determined by simulations on the ns time scale. Therefore, the only quantitative statement that we can make is that both translational and rotational diffusivities drop by significantly as we cross the solid-segment affinity

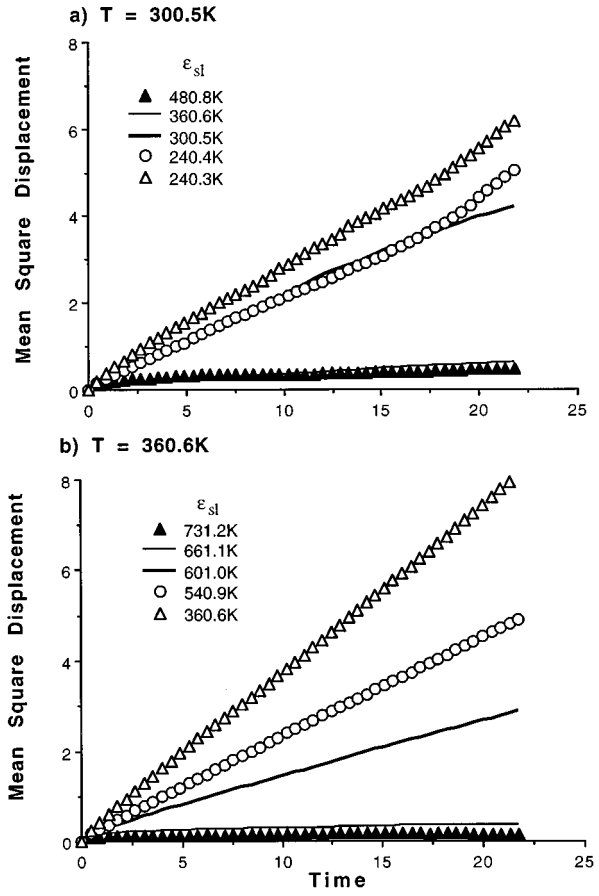

FIG. 6. Chain center of mass mean square displacement parallel to the surface, in the surface layer. The ordinate has been scaled by the radius of gyration (in one direction) of bulk octane. The curves for the higher ϵ_{sl} are very close to the abscissa, indicating a solidlike behavior. The sharp change in the displacement is evident in both the cases.

threshold. Above the critical ϵ_{sl} values, translational and rotational diffusivities dropped by a factor of at least 15 for both temperatures studied. Unfortunately, our limited duration simulations can only provide a lower limit for the decrease of self-diffusion coefficients, but they cannot determine the exact magnitude of this decrease in molecular mobility.

IV. DISCUSSION

In this section we discuss further our findings and examine some of their implications. We also comment on the relation between the simulated systems and actual thin films studied experimentally.

We start with a closer examination of the ordered phases that appear above the critical ϵ_{sl} values. Figure 8 contains typical snapshots of first layer configurations at four different ϵ_{sl} values: $\epsilon_{sl}=180.3$ K, 300.5 K, 360.6 K, 480.8 K at the temperature of 300.5 K. These ϵ_{sl} values include the two immediately below and immediately above the transition threshold. Similar snapshots from the middle layer at the low temperature and from both first and middle layers at the high temperature exhibit very similar features.

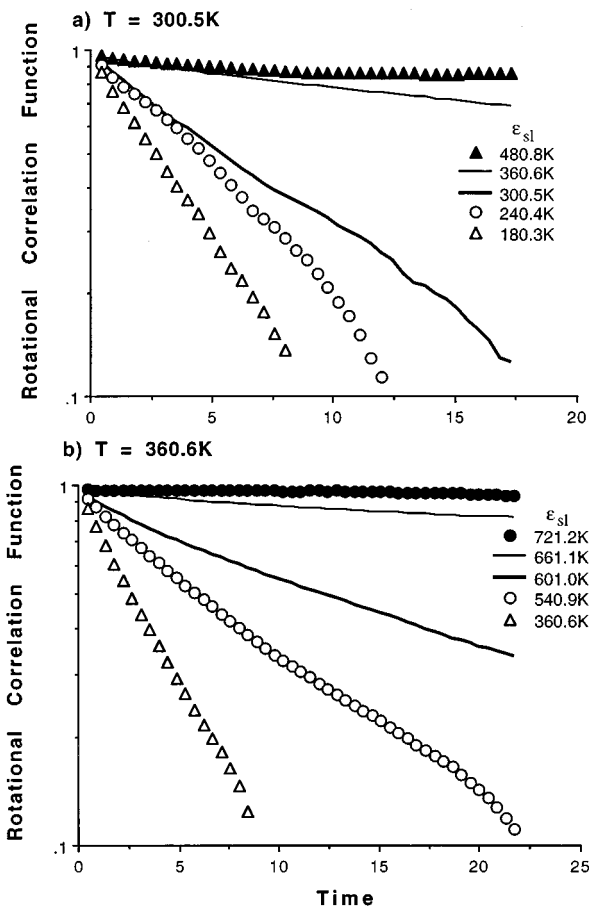

FIG. 7. The rotational correlation function of the octane chains in the film illustrating a decrease at the transition values of ϵ_{sl}.

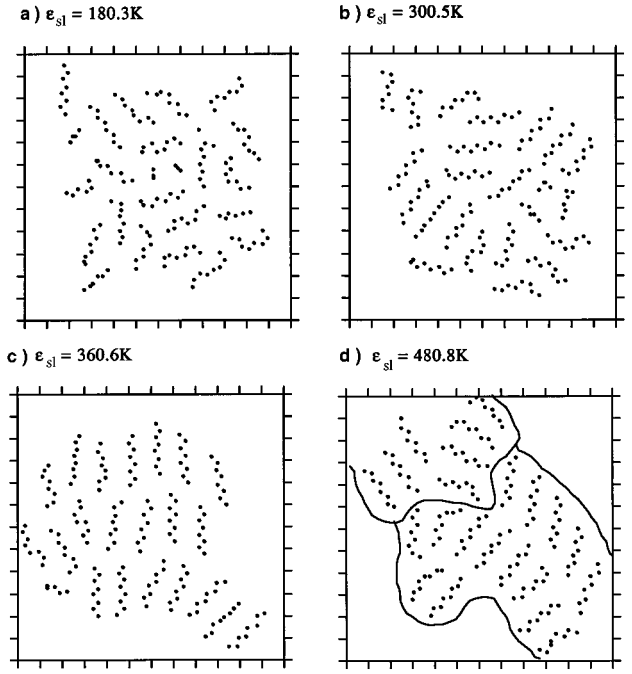

FIG. 8. ''Snapshots'' (projection on the plane parallel to surface) of first layer octane chains for $T=300.5$ K. The distance between ticks on axes represents one methylene unit diameter. Some chains seem to have fewer than eight segments because they are not fully in the first layer. We see a sudden ordering of the chains between $\epsilon_{sl}=300.5$ K and $\epsilon_{sl}=360.6$ K and formation of stable microdomains.

One conspicuous characteristic of the most ordered configuration [Fig. 8(d)] is the presence of two clearly distinguishable domains with their directors roughly perpendicular to each other. The formation of two such domains was apparent in many ordered phases. Domains were stable on the time scale of our simulations (1–2 ns). The presence of ordered domains, instead of a uniform ordered phase, lead to the creation of two ''grains'' throughout the whole film. Each grain typically contained 20–45 octane molecules. Simulations of smaller systems with a periodic dimension of 6σ always lead to the formation of a uniform ordered phase. Therefore, we can conclude that the linear dimension of the domains should be intermediate between 6σ and the periodic dimension of the films discussed in this paper (9σ), i.e., between 2 and 3 nm. This is remarkably close to the domain size inferred from scanning tunneling microscopy experiments of oligomer monolayers deposited on metal surfaces.[12,13] However, it is possible that domains are frozen metastabilities, which cannot relax on the ns time scale. A reliable resolution of this issue by molecular simulations is extremely difficult, if not impossible. Nevertheless, if such a finding could be trusted, its implications on the material properties of thin films would be profound.

A comparison between the first layer (Fig. 3) and middle layer (Fig. 4) pair correlation function curves shows that the middle layer exhibits more structural order above the transition. Although this might appear counterintuitive, it can be explained by examining the structure of the confining surfaces of each layer. Above the transition, the solidlike first layer is sandwiched between a topographically neutral (geometrically flat) and a topographically commensurate middle layer. However, the middle layer is sandwiched between two topographically commensurate surfaces. We believe that this is what leads to a higher degree of order in the middle layer.

Up to this point we avoided using the term ''crystalline'' for the ordered phases. Since octane chains adopt rodlike configurations the ordered phase could in principle be nematic, smectic, or crystalline. More precisely, the above terms correspond to the possible type of intralayer order, i.e., they are used to describe layers, which are two-dimensional entities. It is clear from the snapshots above the transition threshold [Figs. 8(c) and 8(d)] that domains possess a high degree of orientational order. Furthermore, there is a considerable degree of translational order perpendicular to the molecular end-to-end vector. This is also apparent from the well-developed second and third intermolecular nearest neighbor peaks in the pair correlation functions (Figs. 3 and 4). These two features combined already constitute a two-dimensional smectic phase.

A *n*-octane crystal would also possess order in the direction parallel to the chain end-to-end vector resulting from the slight ''roughness'' of the molecular ''texture.'' Such an ordering cannot be seen in the snapshots of Figs. 8(c) and 8(d)

and analogous features in the pair correlation function are absent (Figs. 3 and 4). Therefore, our ordered phases are just short of being crystalline octane. They are also slightly different from the well-known ''rotator'' phases of solid alkanes. In actuality, they are more ordered than ''rotator'' phases, as the molecular skeleton is almost parallel to the solid surfaces, i.e., the rotational invariance with respect to the end-to-end axis is broken. When all of these observations are put together one can safely characterize the ordered domains as solids; they could still possibly undergo a solid–solid phase transition to a fully crystalline *n*-octane film.

Furthermore we did not observe any ''tilting'' transition, corresponding to an abrupt reorientation of the chain skeleton, like that reported in our simulations with atomically rough surfaces.[25] This remark underlines the subtle role of surface topography in determining the exact nature of the thin film.

We have argued that above the transition the film can be safely characterized as solid (or, at worst, a granular solid) or ''polycrystalline.'' Nevertheless, it is a poorly organized solid [Fig. 8(c)], as manifested by the presence of a few large defects (i.e., entire chains) and numerous small defects (i.e., gauche sequences of ordered chains). Again, we should mention that frozen metastabilities, which could persist throughout the duration of our simulations, might undermine the degree of order of the solid phase.

Immediately below the transition the film is a liquid, by any reasonable definition of the term. The strongest argument in support of this statement is molecular mobility, which allows entire octane chains to migrate and rotate on the time scale of 20–40 ps (Figs. 6 and 7). However, it is a much more ''viscous'' and considerably more ''ordered'' liquid than bulk octane. Figure 8(b) illustrates the strong intermolecular correlations just below the transition ($\epsilon_{sl}=300.5$ K), as well as the relatively extended configurations of octane molecules, which facilitate the ordering. More quantitative support for the unusually high order of the liquid phase is the presence of a clearly distinguishable second intermolecular nearest neighbor peak in the pair correlation functions (Figs. 3 and 4) below the transition. This feature is absent from the pair correlation functions of bulk *n*-decane under analogous thermodynamic conditions.[37,38]

Our simulation findings report a liquid-to-solid phase transition. They establish that this is a first order phase transition, since it is characterized by abrupt structural and dynamical changes. They also quantify the transition as a mild one, at least compared to liquid–solid transitions in the bulk, as it transforms a highly ordered liquid to a poorly organized solid.

Conventional phase transitions are the result of changes in thermodynamic conditions. Here we deal with transitions that were caused by solid-segment affinity, a ''molecular'' rather than a thermodynamic quantity. Clearly, the ''macroscopic'' state of molecularly thin films cannot be specified by ''thermodynamic'' variables only, as solid–liquid molecular interactions affect, or even dominate, the film's macroscopic properties. However, the similarity with conventional phase transitions is striking, and the implications of drawing such an analogy are far reaching.

The findings reported in this paper show that thin films of short alkane molecules confined between atomically smooth solid surfaces will exhibit either solid or liquid behavior depending on the type of confining surfaces, and that there do not exist smooth surfaces that produce intermediate behavior. Therefore, they show that atomically smooth solid substrates fall in one of two distinct categories; those that solidify the film and those that do not. There is no gradual evolution from liquidlike to solidlike films for the type of molecules studied in this work.

Furthermore, our simulations establish that solidification of thin films does not require the aid of topography. This provides a natural explanation for the numerous experiments that reported solidlike features of thin films, despite the lack of commensurability between the molecules of the liquids used and the topography of mica substrate.

However, we should add a word of caution concerning the effect of surface topography (which was outside the scope of this study). Although gradual increase of ''adhesiveness'' of atomically smooth surfaces produces sharp (''phase'') transitions in the molecular structure and mobility of the confined film, one cannot rule out the full suppression of such transitions when solid topography is highly incommensurate with that of the film molecules. By the same token, highly commensurate solids will be expected to enhance further the sharpness of energetically (''adhesion'') driven transitions.

Finally, we comment on the relation between simulated systems and systems studied experimentally. The cleavage plane of mica used in the surface force apparatus experiments is a highly adhesive surface. Estimates of its effective ϵ_{sl} range from 360 K to 600 K,[15] which places it above our transition threshold for the ''room conditions'' simulations, i.e., the low temperature, low pressure systems. According to our simulations, the ϵ_{sl} threshold for the liquid-to-solid transition is 330 K at these thermodynamic conditions. This is very likely an overestimate of the actual critical ϵ_{sl} value of thin octane films. Furthermore, these considerations ignore the possibility of a monolayer of water being irreversibly attached on the cleavage plane of mica, which would raise the effective ϵ_{sl} considerably. Such a monolayer of water, or metal oxides, would suffice to bring metal surfaces, which in themselves are slightly below the threshold (250 K),[39] above the critical ϵ_{sl} values for film solidification.

V. SUMMARY

In this paper we presented findings from molecular dynamics simulations designed to explore the nature of changes in thin *n*-octane films as a result of increasing solid-methylene energetic affinity. The solid surfaces were deprived of any topographical features and were modeled as atomically smooth 10-4 Lennard–Jones planes. Two series of simulations were carried out, both under conditions of thermodynamic equilibrium with a different bulk reservoir. The two reservoirs represented markedly different thermody-

namic states of bulk liquid *n*-octane, one being at room temperature and pressure and the other being at an elevated temperature and an extremely high pressure.

In both series of simulations we observed an abrupt transition in the structural features of the film at some critical value of the characteristic energy that quantified the affinity between the solid surfaces and the methylene units. The transition was signaled by a discontinuous increase of intermolecular ordering reflected in the development of strong, well-defined second and third intermolecular neighbor peaks in the pair correlation function. The transition was facilitated by a precipitous extension of the octane molecules, which adopted almost fully extended, all trans configurations. Furthermore, it resulted in the freezing of large scale molecular migration and rotation.

The characteristics of the transition showed that it is a first order phase transition, albeit a relatively mild one, as it transformed a highly ordered liquid to a poorly organized solid. The solid constituted a phase with order intermediate between that of hydrocarbon ''rotator'' phases and two-dimensional smectics.

These findings demonstrate that solidification of nanoscopically thin films of linear alkanes, under conditions where the bulk material is a liquid, is a generic, energetically driven phenomenon. The solidification does not require the aid of a commensurate surface topography, although it may be promoted or suppressed by topographical features of the confining surfaces. Its close analogy with conventional phase transitions suggests that the vast majority of confining surfaces will belong to two distinct categories: those that preserve the liquidlike properties of the film and those that induce its solidification. At least for short linear alkane films confined between atomically smooth surfaces there do not exist smooth surfaces that produce an intermediate behavior.

Our simulation findings provide a natural explanation for the solidlike features of nanoscopically thin linear alkane films studied experimentally. Furthermore, they show that the cleavage plane of mica, which is the most commonly used confining surface in these experiments, is certainly adhesive enough to induce solidification of the confined film and can do so without being topographically commensurate with the molecules of the confined film.

ACKNOWLEDGMENTS

Financial support for this work was provided by NSF (Grant No. CTS-9015882) and the Department of Chemical Engineering at the University of Florida.

[1] A. M. Homola, G. B. Street, and C. M. Mate, MRS Bulletin, **XV(3)**, 45 (1990).
[2] M. M. Denn, Annu. Rev. Fluid Mech. **22**, 13 (1990).
[3] D. Tabor and R. H. S. Winterton, Proc. R. Soc. London, Ser. A **312**, 543 (1969); J. N. Israelachvili, and D. Tabor, *ibid.* **331**, 19 (1972); J. N. Israelachvili, and G. E. Adams, J. Chem. Soc. Faraday Trans. I **74**, 975 (1978).
[4] J. N. Israelachvili, P. M. McGuiggan, and A. M. Homola, Science **240**, 189 (1988).
[5] J. van Alsten and S. Granick, Phys. Rev. Lett. **61**, 2570 (1988).
[6] A. M. Homola, H. V. Nguyen, and G. Hadziioannou, J. Chem. Phys. **94**, 2346 (1991).
[7] J. N. Israelachvili, P. M. Mc Guiggan, and A. M. Homola, Science **240**, 189 (1988).
[8] S. Granick, Science **253**, 1374 (1991).
[9] D. Y. Chan and R. G. Horn, J. Chem. Phys. **83**, 5311 (1985).
[10] A. D. Nikolov and D. T. Wasan, J. Coll. Inter. Sci. **133**, 1 (1989); **133**, 13 (1989).
[11] A. D. Nikolov, D. T. Wasan, N. D. Denkov, P. A. Kralchesvky, and I. B. Ivanov, Prog. Coll. Pol. Sci. **82**, 1 (1990).
[12] J. P. Rabe and S. Buchholz, Phys. Rev. Lett. **66**, 2096 (1991).
[13] R. Hentske, B. L. Schurmann, and J. P. Rabe, J. Chem. Phys. **92**, 6213 (1992).
[14] T. K. Knudstrup, I. A. Bitsanis, and G. B. Westermann-Clark, Langmuir **11**, 893 (1995).
[15] J. Peanasky, L. L. Cai, and S. Granick, Langmuir **10**, 3874 (1994).
[16] J. J. Magda, M. Tirrell, and H. T. Davis, J. Chem. Phys. **83**, 1888 (1985).
[17] I. Bitsanis, J. J. Magda, M. Tirrell, and H. T. Davis, J. Chem. Phys. **87**, 1733 (1987).
[18] I. Bitsanis, S. A. Somers, H. T. Davis, and M. Tirrell, J. Chem. Phys. **93**, 3427 (1990).
[19] M. Schoen, J. H. Cushman, D. J. Diestler, and C. L. Rhykerd, Jr., J. Chem. Phys. **88**, 1394 (1988).
[20] P. A. Thompson and M. O. Robbins, Phys. Rev. A **41**, 6830 (1990).
[21] P. A. Thompson, G. S. Grest, and M. O. Robbins, Phys. Rev. Lett. **68**, 3448 (1992).
[22] I. A. Bitsanis and C. Pan, J. Chem. Phys. **99**, 5520 (1993).
[23] T. K. Xia, J. Quyang, M. W. Ribarsky, and U. Landman, Phys. Rev. Lett. **69**, 1967 (1992).
[24] S. Gupta, D. C. Koopman, G. B. Westermann-Clark, and I. A. Bitsanis, J. Chem. Phys. **100**, 8444 (1994).
[25] D. C. Koopman, S. Gupta, R. K. Ballamudi, G. B. Westermann-Clark, and I. A. Bitsanis, Chem. Eng. Sci. **49**, 2907 (1994).
[26] J. P. Ryckaert and A. Bellemans, Faraday Discuss. Chem. Soc. **66**, 95 (1978).
[27] S. Toxvaerd, J. Chem. Phys. **93**, 4290 (1990); P. Padilla, and S. Toxvaerd, *ibid.* **94**, 5650 (1991).
[28] T. A. Weber, J. Chem. Phys. **69**, 2347 (1978); **70**, 4277 (1979).
[29] M. P. Allen and D. J. Tildesley, *Computer Simulation of Liquids* (Oxford, New York, 1989).
[30] J. P. Ryckaert, G. Ciccotti, and H. L. C. Berendsen, J. Comput. Phys. **23**, 327 (1977).
[31] N. G. van Kampen, *Stochastic Processes in Physics and Chemistry* (North Holland, Amsterdam, 1981).
[32] M. Fixmann, J. Chem. Phys. **69**, 1527 (1978).
[33] N. G. van Kampen, Appl. Sci. Res. **37**, 67 (1981).
[34] J. A. Mongomery, Jr., S. L. Holmgren, and D. Chandler, J. Chem. Phys. **73**, 3688 (1980).
[35] D. Rigby and R. J. Roe, J. Chem. Phys. **87**, 7285 (1987).
[36] D. Nicholson and N. G. Parsonage, *Computer Simulation and the Statistical Mechanics of Adsorption* (Academic, New York, 1982).
[37] S. Gupta, G. B. Westermann-Clark, and I. Bitsanis, J. Chem. Phys. **98**, 634 (1993).
[38] R. Edberg, D. J. Evans, and R. J. Moriss, J. Chem. Phys. **84**, 6933 (1986).
[39] A. V. Hamza and R. J. Madix, Surf. Sci. **179**, 25 (1987).